Cement and Concrete Research 41 (2011) 571–578

Contents lists available at ScienceDirect

Cement and Concrete Research

journal homepage: http://ees.elsevier.com/CEMCON/default.asp

Pressure induced reactions amongst calcium aluminate hydrate phases

Ju-hyuk Moon [a], Jae Eun Oh [b], Magdalena Balonis [c], Fredrik P. Glasser [c], Simon M. Clark [d,e], Paulo J.M. Monteiro [a,*]

[a] Department of Civil and Environmental Engineering, University of California, Berkeley, CA 94720, USA
[b] School of Urban and Environmental Engineering, Ulsan National Institute of Science and Technology, Ulsan Metropolitan City, 689-798, South Korea
[c] Department of Chemistry, Meston Building, University of Aberdeen, Aberdeen, AB24 3UE Scotland, UK
[d] Advanced Light Source, Lawrence Berkeley National Laboratory, Berkeley, CA20015, USA
[e] Department of Earth and Planetary Sciences, University of California, Berkeley, CA94720, USA

ARTICLE INFO

Article history:
Received 10 December 2010
Accepted 11 February 2011

Keywords:
X-ray diffraction (B)
High pressure
Elastic moduli (C)
Hydrogarnet (D)
Calcium aluminate hydrates (D)

ABSTRACT

The compressibilities of two AFm phases (strätlingite and calcium hemicarboaluminate hydrate) and hydrogarnet were obtained up to 5 GPa by using synchrotron high-pressure X-ray powder diffraction with a diamond anvil cell. The AFm phases show abrupt volume contraction regardless of the molecular size of the pressure-transmitting media. This volume discontinuity could be associated to a structural transition or to the movement of the weakly bound interlayer water molecules in the AFm structure. The experimental results seem to indicate that the pressure-induced dehydration is the dominant mechanism especially with hygroscopic pressure medium. The Birch–Murnaghan equation of state was used to compute the bulk modulus of the minerals. Due to the discontinuity in the pressure–volume diagram, a two stage bulk modulus of each AFm phase was calculated. The abnormal volume compressibility for the AFm phases caused a significant change to their bulk modulus. The reliability of this experiment is verified by comparing the bulk modulus of hydrogarnet with previous studies.

1. Introduction

During the hydration of Portland cement, AFm (Al_2O_3–Fe_2O_3-mono) phases are formed when ions are brought together in appropriate concentrations in aqueous systems at room temperature or formed hydrothermally, i.e. in the presence of water under pressure above 100 °C. They are among the hydration products of Portland cements. AFm phases have layer structures derived from that of portlandite, $Ca(OH)_2$, whereby one third of Ca^{2+} ions are replaced by a trivalent ion, nominally Al^{3+} or Fe^{3+} ion. The principal layer has the chemical formula $[Ca_2(Al,Fe)(OH)_6]^+$. Between the principal layer it includes charge-balancing X anions and water molecules [1]. This interlayer region has the composition $[X_nH_2O]^-$. The X anion could be hydroxide, sulfate, chloride, or carbonate. The layer thickness c′ depends on the nature of the X anion and the amount of interlayer water, which can be varied by stepwise dehydration at different temperature and humidity conditions [1–3].

One AFm phase, dicalcium aluminate monosilicate-8-hydrate $Ca_2Al_2SiO_7 \cdot 8H_2O$, trigonal, R3, R3 or R3m (also called gehlenite hydrate) occurs in nature as strätlingite [4–7]. Its interlayer content is $[AlSi(OH)_8 \cdot H_2O]^-$; the Al is tetrahedrally coordinated [8]. This phase appears in the hydration of slag-containing Portland cements or blended cements and contributes to compressive strength development in commercial high alumina cement [9].

Another AFm phase is tetracalcium aluminate hemicarbonate-12-hydrate (also called hemicarboaluminate), $Ca_4Al_2(CO_3)_{0.5}(OH)_{13} \cdot 5.5H_2O$, trigonal, R3c or R3c system [6,10]. This phase occurs in ordinary Portland cement with very low carbonate contents. There are two types of carbon-containing AFm phases: CO_3^{2-} anion monocarboaluminate (C_4ACH_{11}, triclinic, P1 system [11]) and hemicarboaluminate ($C_4AC_{0.5}H_{12}$). At ambient conditions, monocarboaluminate and hemicarboaluminate have $[1/2(CO_3^{2-}) \cdot 5/2H_2O]^-$ and $[1/4(CO_3^{2-}) \cdot 1/2(OH^-) \cdot 11/4H_2O]^-$ as interlayer contents, respectively. The interlayer contents and layer thickness of hemicarboaluminate at varying hydration stages were studied by Fischer and Kuzel [10] and are shown in Table 1.

Changes in the water content associated with concomitant relaxation of the AFm framework have been observed in numerous variable-temperature studies, which explains why AFm phases undergo several dehydration stages at higher temperatures (see Table 1). The effects of pressure on the structure and the detailed crystal properties of dehydrated AFm phases are less well explored. Recently, Clark et al. calculated the bulk modulus of ettringite—one of AFt phases—using X-ray and infrared study [12]. But for AFm phases that are often less stable compared to the AFt phase, high-pressure structural data are not yet available.

During synthesis of AFm phases, the low stability of hydroxyl AFm results in the appearance of other phases in the course of synthesis,

* Corresponding author.
E-mail address: monteiro@berkeley.edu (P.J.M. Monteiro).

0008-8846/$ – see front matter © 2011 Elsevier Ltd. All rights reserved.
doi:10.1016/j.cemconres.2011.02.004

Table 1
Dehydration stages for AFm phases and crystal information.

		Space Group		Layer thickness (Å)	a (Å)	c (Å)	V (Å^3)	
Strätlingite	C_2ASH_8	R3, R3	27 °C 37% RH	12.55	5.747	37.64	1076.62	[5]
			27 °C	–	5.737	37.59	1071.45	[4]
			27 °C	–	5.745	37.77	1079.59	[5]
			30 °C	–	5.747	37.638	1076.56	[6]
	C_2ASH_4	–	>135 °C	11.2	–	–	–	[5]
	$C_2ASH_{7.25}$	R3m	27 °C	–	5.745	37.77	1079.59	[7]
Hemicarbo aluminate	$C_4AC_{0.5}H_{12}$	R3c, R3c	22 °C 36% RH	8.193	5.770	49.159	1417.37	[10]
			30 °C	–	5.761	49.252	1415.63	[6]
	$C_4AC_{0.5}H_{11.25}$	–	35 °C	7.63	–	–	–	[10]
	$C_4AC_{0.5}H_{10.5}$	–	80 °C	7.26	–	–	–	
	$C_4AC_{0.5}H_{6.5}$	–	105 °C	6.6	–	–	–	
Hydrogarnet	C_3AH_6	IA–3D	27 °C	–	12.576	–	1988.73	[13]
			–	–	12.56	–	1981.39	[14]
			27 °C	–	12.57	–	1985.89	[15]

notably hydrogarnet with hemicarboaluminate [13–15]. Hydrogarnet, $Ca_3Al_2(OH)_{12}$, cubic, Ia3d, whose structure is related to that of grossularite garnet [3], appears more readily in nominally sulfate-free cements. However, it is strongly destabilized by sulfate at low temperatures, (<50 °C) thus it does not generally appear in Portland cement unless the cement has been heat cured. Due to its importance in geophysics, the behavior of hydrogarnet under pressure has been well studied [16–20].

The title study reports the behavior of the AFm phases, strätlingite and hemicarboaluminate and hydrogarnet (with hemicarboaluminate as a minor phase) under pressure using diamond anvil cell and high-pressure synchrotron X-ray diffraction. Also, the bulk moduli of AFm phases and hydrogarnet are computed and compared with previous studies.

2. Experimental procedure

All AFm samples were synthesized following the methods of Matschei et al. [21]. High pressures were generated using a diamond anvil cell. Ambient condition phase identification and the high-pressure powder X-ray diffraction experiment were carried out at beamline 12.2.2 of the Advanced Light Source [22], using a synchrotron monochromatic X-ray beam. The wavelength of the beam was different depending on the energy status of the beamline

Table 2
Experimental pressures and measured lattice parameters and unit cell volumes.

	P (GPa)	a (Å)	c (Å)	V (Å^3)
Strätlingite	Ambient	5.754(7)	37.56(1)	1077.30(2)
Pressure medium: silicone oil	0.1(1)	5.75(1)	37.56(1)	1075.57(3)
Wavelength: 0.6199 Å	0.8(2)	5.697(5)	36.887(4)	1036.96(1)
Sample-to-detector distance: 401.1380 mm	1.5(2)	5.669(5)	36.678(5)	1020.99(1)
	2.2(2)	5.654(3)	36.603(3)	1013.43(1)
	2.9(3)	5.646(4)	36.480(4)	1007.16(1)
	3.4(3)	5.638(2)	36.456(3)	1003.72(1)
Hemicarboaluminate	Ambient	5.770(2)	49.181(5)	1418.04(1)
Pressure medium: silicone oil	0.1(1)	5.771(1)	49.222(9)	1419.98(1)
Wavelength: 0.4959 Å	0.5(1)	5.754(9)	48.29(4)	1385.1(3)
Sample-to-detector distance: 292.9597 mm	1.1(2)	5.74(8)	46.3(3)	1323.8(2)
	2.4(2)	5.70(8)	45.0(3)	1270.7(3)
	3.6(3)	5.6(1)	43.9(4)	1232.3(3)
	5.4(4)	5.6(1)	43.3(4)	1205.0(3)
Hemicarboaluminate	Ambient	5.765(8)	49.28(5)	1418.94(4)
Pressure medium: 4:1 methanol:ethanol	0.1(1)	5.774(6)	48.92(4)	1412.68(3)
Wavelength: 0.4133 Å	0.9(2)	5.750(1)	46.3(3)	1326.9(2)
Sample-to-detector distance: 400.8096 mm	1.8(2)	5.71(8)	45.2(3)	1279.3(3)
	3.4(3)	5.69(9)	44.0(4)	1237.0(3)
	3.8(3)	5.6(1)	43.7(5)	1217.5(4)
	4.2(4)	5.6(1)	43.6(5)	1211.3(4)
Hydrogarnet	Ambient	12.57(1)	–	1984.51(7)
Pressure medium: silicone oil	0.1(1)	12.561(8)	–	1982.38(1)
Wavelength: 0.4959 Å	0.5(1)	12.53(5)	–	1968.62(5)
Sample-to-detector distance: 292.9597 mm	1.1(2)	12.50(1)	–	1954.48(1)
	2.4(2)	12.44(2)	–	1928.98(2)
	3.6(3)	12.37(7)	–	1896.45(7)
	5.4(4)	12.2(1)	–	1851.0(1)
Hydrogarnet	Ambient	12.57(1)	–	1987.11(1)
Pressure medium: 4:1 methanol:ethanol	0.1(1)	12.51(7)	–	1959.01(7)
Wavelength: 0.4133 Å	0.9(2)	12.50(6)	–	1956.03(7)
Sample-to-detector distance: 400.8096 mm	1.8(2)	12.46(2)	–	1935.65(3)
	3.4(3)	12.38(3)	–	1898.42(3)
	3.8(3)	12.377(8)	–	1896.13(1)

Note: Standard deviations in parentheses.

(see Table 2). The National Bureau of Standards LaB_6 powder diffraction standard was used to calibrate the working distance between the sample and detector (see Table 2). Diffraction patterns were collected using a MAR345 image plate (3450×3450 pixels).

All samples were finely ground and mixed with a pressure medium and a few chips of ruby in a glove box to avoid carbonation [21]. Samples were placed into a sample chamber comprising a steel gasketed diamond anvil cell. The sample chamber size was 180-μm diameter, with 75-μm thickness. The pressure was controlled by two screws of the diamond anvil cell. The sample was equilibrated for about 20 min. at each pressure. Exposure times of 300 s were sufficient to give adequate signals for powder diffraction patterns. For strätlingite, silicone oil (a mixture composed of polysiloxane chains with methyl and phenyl groups) was used as the pressure medium. For hemicarboaluminate, silicone oil was used in the first run and a 4:1 mixture of methanol:ethanol for the second run. For all experiments diffraction patterns were collected with incremental rising and falling pressure. The pressure was measured at off-line using the ruby fluorescence technique [23]. All two-dimensional X-ray data were radially integrated to give powder diffraction patterns using the fit2d program [24].

3. Results

3.1. Strätlingite, $Ca_2Al_2SiO_7 \cdot 8H_2O$

The ambient X-ray diffraction pattern and high-pressure patterns of strätlingite are shown in Fig. 1. The position and relative intensities of X-ray reflections of the strätlingite agree with the data of Kuzel [5] and Rinaldi et al. [7]. Newly emerging peaks observed in the post-compression sample were due to the steel gaskets and ruby chips which were present during the collection of the post-compression pattern while they were absent at ambient conditions. Diffraction peak positions of (003), (006), (009), (110), and (021) were used to calculate the unit cell volume of strätlingite. Changes in lattice parameters and a unit cell volume of the samples were calculated using the software XFit [25] and Celref program [26] (see Table 2). The calculated lattice parameters as a function of pressure is shown in Fig. 2. The sample was found to irreversibly transform to an amorphous phase at 3.4 GPa.

The pressure-normalized volume data was fitted by a Birch–Murnaghan equation of state (B.M. EoS) (Table 3). In the relationship of F versus f in B.M. EoS, the y-intercept and slope of the weighted least-squares fit provide the bulk modulus K_o and its derivative K_o'

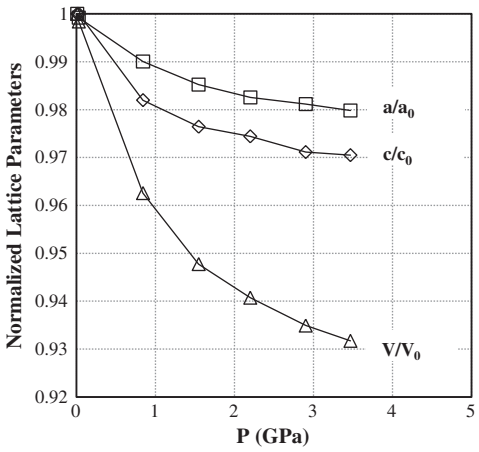

Fig. 2. Unit cell parameters and volume of strtlingite normalized to ambient values as a function of pressure.

[27]. A weighted linear least-squares fit with errors was applied to this study to consider both pressure and volume errors [28]. Due to its abnormal compressibility, the bulk modulus of strätlingite was calculated in two pressure ranges of 0.1–1.5 GPa and 1.5–3.4 GPa. In the second pressure range, the initial volume for B.M. EoS at the point of the convergence was estimated at a value of 1035.67 $Å^3$ [29]. Finally, the bulk modulus K_o and its derivative K_o' were calculated with $R^2 = 0.978$ and 0.996 fitting convergence, shown in Fig. 3. At the first pressure stage, because the number of volume–pressure points was too small to get a reasonable K_o' value, the value of K_o' was fixed at 4.0. The compressibility data for the B.M. EoS yielded a bulk modulus of $K_o = 23(2)$ and 100(3) GPa from 0.1 to 1.5 GPa and from 1.5 to 3.4 GPa, respectively.

3.2. Calcium hemicarboaluminate hydrate, $Ca_4Al_2(CO_3)_{0.5}(OH)_{13} \cdot 5.5H_2O$

Figs. 4 and 5 show the whole X-ray diagram stack of hemicarboaluminate with different pressure-transmitting media. The reflection data for hemicarboaluminate agreed with the data obtained by Fischer and Kuzel [10]. Matschei et al. suggested that monocarboaluminate and hydrogarnet could be found coexisting with hemicarboaluminate [21]. Also with rising temperature, the high temperature formation of portlandite in stoichiometric mixtures arises from the increasing destabilization of hemicarboaluminate.

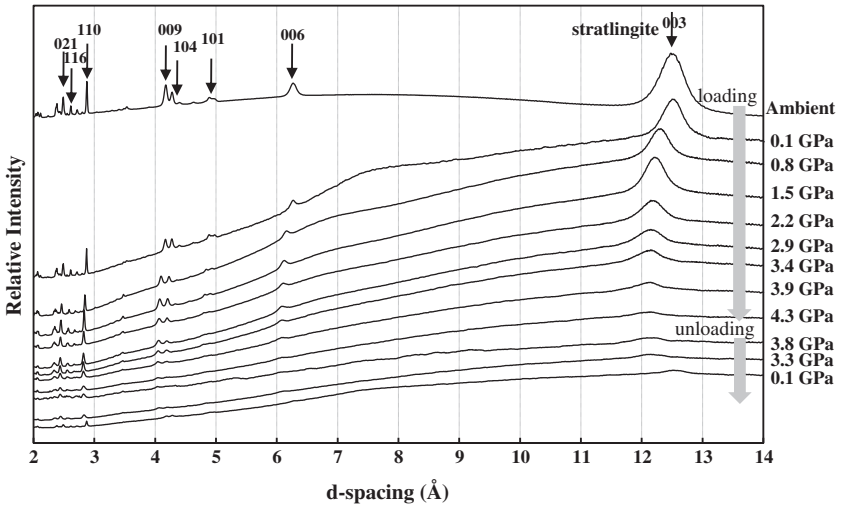

Fig. 1. Integrated powder X-ray diffraction patterns of strtlingite as a function of pressure, where the pattern with a label of 'Ambient' was taken at ambient X-ray diffraction and the others through DAC with silicone oil pressure-transmitting medium.

Table 3
Bulk modulus, its first derivative (calculated K_o and fixed $K_o' = 4$) and ambient cell volume according to the third-order Birch–Murnaghan equation of state.

	Pressure transmitting medium	Pressure range (GPa)	Initial volume (Å^3)	K_o'	K_o (GPa)	$K_o' =$ fixed	K_o (GPa)
Strätlingite	Silicone oil	0.1–1.5	1077.30(2)	n.d.	n.d.	**4**	**23(2)**
		1.5–3.4	1035.67*	3.8	100(11)	**4**	**100(3)**
Hemicarboaluminate	Silicone oil	0.1–1.1	1418.04(1)	n.d.	n.d.	**4**	**15(2)**
		1.1–5.4	1361.25*	4.19	32(7)	**4**	**32(2)**
	Methanol:ethanol = 4:1	0.1–1.8	1418.94(4)	13.6	9(2)	**4**	**14(1)**
		1.8–4.2	1351.57*	4.0	30(3)	**4**	**31(1)**
Hydrogarnet	Silicone oil	0.1–5.4	1984.51(7)	1.4	77(5)	**4**	**72(4)**
	Methanol:ethanol = 4:1	0.1–3.8	1987.11(1)	13.5	58(5)	**4**	**69(4)**

Note: n.d.: not determined, * Estimated initial volume for the convergence of bulk modulus in dehydrated phase [29].

However, some differences of basal reflections which are not consistent with those of monocarboaluminate or portlandite at ambient pressure can be explained by the different water contents in the interlayer of the hemicarboaluminate. In the hemicarboaluminate the dehydration is very likely to happen as indicated by relatively low temperature of dehydration (see Table 1). The layer thicknesses of 8.193 Å of $C_4AC_{0.5}H_{12}$ and 7.63 Å of $C_4AC_{0.5}H_{11.25}$ agree with those of the ambient diffraction patterns [10], indicating that both $C_4AC_{0.5}H_{12}$ and $C_4AC_{0.5}H_{11.25}$ coexist in the ambient sample. Fig. 6 shows raw 2-dimensional powder diffraction pattern corresponding to basal spacing of a hemicarboaluminate contained in a diamond anvil cell with 4:1 methanol:ethanol pressure-transmitting medium. As pressure increased, however, those two basal reflections merged together to one intense peak (Fig. 6).

To calculate the volume of hemicarboaluminate, the (006), (018), (110), (119), and (024) peaks were selected. The XFit program [25] was used to define peak positions at each pressure point. The unit cell volume and corresponding volume errors were calculated using the Celref program [26]. Like strätlingite, the hemicarboaluminate also showed abnormal compressibility. To understand the relationship between this abnormal compressibility and the pressure medium, the pressure-transmitting medium was changed to methanol and ethanol, at a volume ratio of 4:1; this is often used in high-pressure research, but it does make it more challenging to load the sample because of its rapid evaporation. The results presented here show that the nature of the pressure-transmitting medium itself does not significantly affect these unusual high-pressure phenomena. The calculated lattice parameters as a function of pressure are given in Fig. 7. Unlike strätlingite, hemicarboaluminate was found to reversibly transform to the initial volume phase with silicone oil as the pressure decreased to ambient.

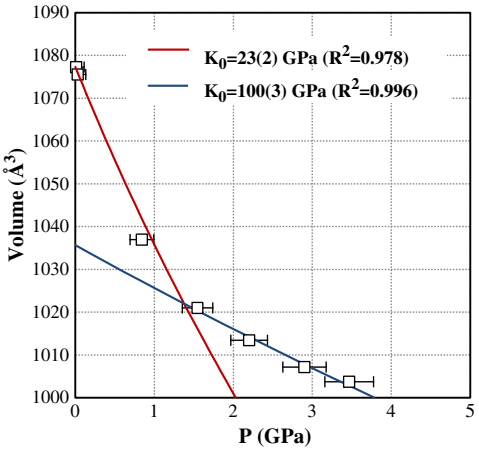

Fig. 3. Unit cell volume as a function of pressure fitted to the B.M. EoS for strtlingite. K_o' is fixed at 4.0. Red line is the fit from 0.1 to 1.5 GPa and blue line is the fit from 1.5 to 3.4 GPa.

For hemicarboaluminate, the compressibility of a/a_0, c/c_0, and volume decreased with increasing hydrostatic pressure (Fig. 7). Again, the pressure range could be divided into two regions. In the second pressure range, the initial volume for B.M. EoS calculation provided values of 1361.25 Å^3 and 1351.57 Å^3 for the silicone oil and the methanol and ethanol solution, respectively. Finally, the compressibility data for the B.M. EoS yielded a bulk modulus of $K_o = 15(2)$ and 14(1) GPa from 0.1 to 1.1 GPa with silicone oil and from 0.1 to 1.8 GPa with the methanol and ethanol solution, respectively (Fig. 8). For the second phase, $K_o = 32(2)$ and 31(1) GPa from 1.1 to 5.4 GPa with silicone oil and from 1.8 to 4.2 GPa with the methanol and ethanol solution, respectively. The obtained bulk modulus is within error limits of standard deviations regardless of the pressure medium.

3.3. Hydrogarnet, $Ca_3Al_2(OH)_{12}$

A small amount of hydrogarnet was observed in the hemicarboaluminate sample (Figs. 4 and 5). Since the crystal structure of hydrogarnet is cubic, it is relatively easy to calculate its unit cell volume in spite of its small quantity. The (211), (321), and (400) peaks were selected for calculation. This volume–pressure result showed a perfect linear relationship over the entire pressure range in both pressure media. The lattice parameters and fitted volume–pressure curve are shown in Figs. 9 and 10. The B.M. EoS accounts well for the sets of data obtained with both silicone oil and methanol and ethanol solution pressure medium, and yielded a bulk modulus $K_o = 69(4)$ and 72(4) with the pressure derivative K_o', fixed at 4.0. In addition, the sample was found to reversibly transform to its initial state.

4. Discussion

Under high pressure, both strätlingite and hemicarboaluminate show a sudden volume contraction around 1.5 GPa. Previous high-pressure studies in materials containing large channels have shown that some pressure-transmitting medium may infiltrate into structural channels and cause a volume discontinuity. These studies have shown that the high-pressure behavior is highly dependent on the molecular size of the pressure-transmitting medium [30]. However abnormal compressibility of AFm phases has not been analyzed yet. To determine the pressure medium effect on the abrupt volume contraction, the behavior of hemicarboaluminate was checked with different pressure media and it was determined that the pressure medium does not affect the abnormal pressure behavior of AFm phases.

Although the ambient sample began with two hydration stages of hemicarboaluminate, these two basal peaks, at 8.193 Å for $C_4AC_{0.5}H_{12}$ and 7.63 Å for $C_4AC_{0.5}H_{11.25}$, merge together into one intense peak under pressure (Figs. 4 and 5). This might be explained if the fully-hydrated hemicarboaluminate ($C_4AC_{0.5}H_{12}$), initially mixed with $C_4AC_{0.5}H_{11.25}$, moves towards $C_4AC_{0.5}H_{11.25}$ once the pressure attains a certain level. Moreover, the basal reflection decreased stepwise to

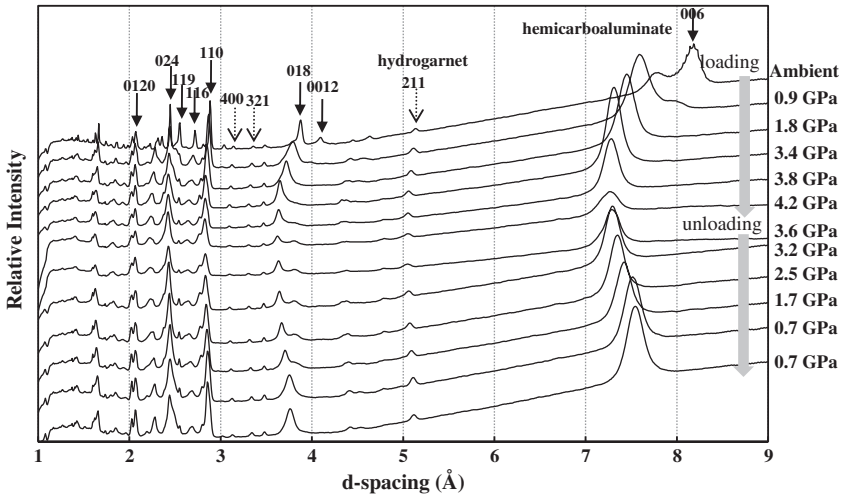

Fig. 4. Integrated powder X-ray diffraction patterns of hemicarboaluminate as a function of pressure, where the pattern with a label of 'Ambient' was taken at ambient X-ray diffraction and the others through DAC with 4:1 methanol:ethanol pressure-transmitting medium.

another hydration stage, i.e. 7.26 Å of $C_4AC_{0.5}H_{10.5}$ (see Table 1), indicating that this might reflect pressure-induced dehydration.

Another possibility is that, with changing pressure, a re-orientation of the carbonate groups occurs. The interchangeable ions in hemicarboaluminate include both OH and CO_3; the planar carbonate groups are assumed to be oriented normal to the plane of the calcium aluminate layer. Because of this orientation, which is not very economical in filling space, Balonis and Glasser noted that its physical density is lower than that of a hypothetical parallel arrangement of planar carbonate groups [6]. In monocarboaluminate, the carbonated group is sub-parallel to the main layer (tilted by 21.8° from the main layers) [11,31]. A pressure-induced change in the orientation of the carbonate group could explain the gradual discontinuity with rising pressure. Unlike strätlingite, perfect-bilinear pressure–volume behavior, hemicarboaluminate shows gradual abnormal pressure-volume behavior. Thus gradual abnormal compressibility of hemicarboaluminate could result from the re-orientation of carbonate groups or from an entirely different cause; pressure-induced dehydration.

To test the two hypotheses, the hemicarboaluminate samples were measured in two different pressure transmitting media: hygroscopic 4:1 methanol:ethanol solution and non-hygroscopic silicone oil. If the re-orientation of carbonate group of hemicarboaluminate is the dominant process, the type of pressure medium should not affect the final structure upon unloading. However, if pressure-induced dehydration is the dominant mechanism the chemical nature of the pressure medium must have a pronounced effect on the crystal structure at ambient pressure when the sample is unloaded because the hygroscopic medium will not allow water to return into the interlayer region while the non-hygroscopic medium would permit the recovery of the original crystal structure once the pressure is removed. Fig. 4 shows the hysteresis of the hemicarboaluminate when a hygroscopic medium is used, while the results given in Fig. 5 indicate that the crystal structure returns to the original state once the sample is unloaded with the non-hygroscopic medium. These experimental results seem to favor the hypothesis that pressure-induced dehydration occurs. Considering the characteristic that the dehydration of hemicarboaluminate is likely happen at 35 °C [6], we can assume that the hygroscopic pressure medium could rapidly extract water molecules from the interlayer region. It could accelerate the pressure-induced dehydration especially at the low pressure range. Fig. 11 shows this hygroscopic medium effect. In the loading process, the layer thickness with hygroscopic medium is slightly smaller than that with non-hygroscopic medium which supports the

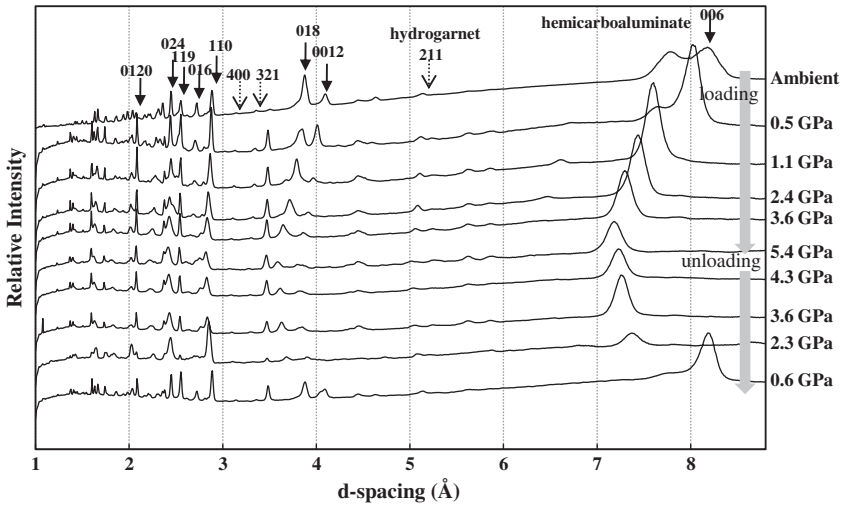

Fig. 5. Integrated powder X-ray diffraction patterns of hemicarboaluminate as a function of pressure, where the pattern with a label of 'Ambient' was taken at ambient X-ray diffraction and the others through DAC with silicone oil pressure-transmitting medium.

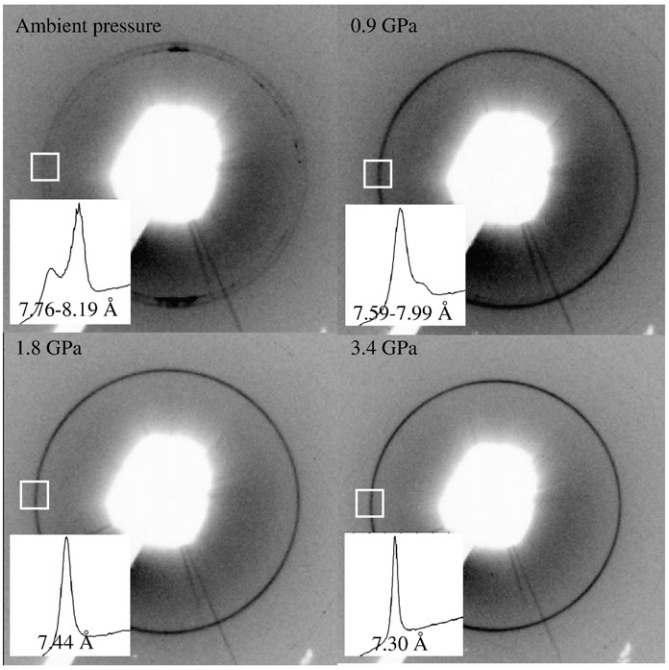

Fig. 6. Raw 2-dimensional powder diffraction pattern corresponding to basal spacing of a hemicarboaluminate contained in a diamond anvil cell with 4:1 methanol: ethanol pressure-transmitting medium.

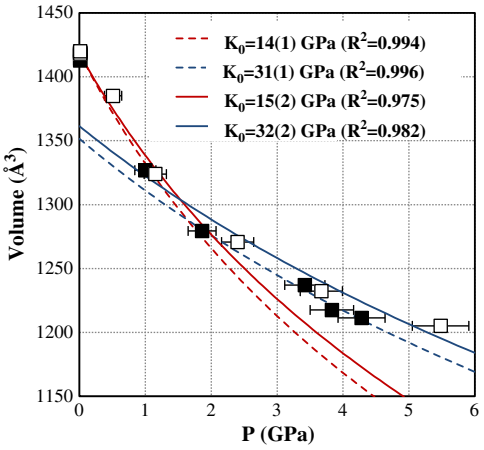

Fig. 8. Unit cell volume as a function of pressure fitted to the B.M. EoS for hemicarboaluminate. K_o' is fixed at 4.0. Red dotted line is the fit from 0.1 to 1.8 GPa; red solid line is the fit from 0.1 to 1.1 GPa; blue dotted line is the fit from 1.8 to 4.2 GPa; and blue solid line is the fit from 1.1 to 5.4 GPa; closed symbols with dotted line and open symbols with solid line correspond to pressure medium of 4:1 methanol:ethanol and silicone oil, respectively.

hypothesis of accelerating dehydration by hygroscopic medium under pressure.

Per formula unit of strätlingite, the interlayer unit ($[AlSi(OH)_8 \cdot H_2O]^-$) contains only one water molecule. Considering the hypothesis of pressure-induced dehydration, the stiffness of the crystal should increase once water molecules move out from the calcium aluminosilicate framework. This phenomenon is confirmed by the experimental results shown in Fig. 3, where an increase in stiffness is observed for pressures greater than 1.5 GPa.

From a mechanical point of view, a noteworthy characteristic of this pressure-induced dehydration is that the frameworks of the crystals are preserved throughout the dehydration. The slight rearrangements of structural elements, even if several weak interlayer water bonds are broken, are not sufficient to destroy the crystal framework of the sample; which transforms from strätlingite to "metasträtlingite". It is possible, therefore, to calculate its bulk modulus at each hydration stage. Based on this assumption, two stage bulk modulus of each hydration stage were calculated. Using the method developed by Jeanloz [29], the initial volume of the second stage at ambient pressure was estimated and regression curve at each stage gave excellent fit.

Although there is still some controversy about the effects of impurities on a high-pressure experiment, a comparison of the reported bulk modulus of hydrogarnet with the results obtained in this study showed agreement within an acceptable error range (see Table 4) [16–20]. Given that the amount of hydrogarnet is very small compared to hemicarboaluminate, the bulk modulus obtained for hydrogarnet is less accurate than values obtained from single-crystal high-pressure experiment [18]. However, since the volume–pressure behavior of hydrogarnet—which is a framework structure not generating interlayer sites—does not show any abnormal compressibility, it is safe to assume that the abnormal compressibility of AFm phases is due to the existence of loosely bonded interlayer water molecules.

5. Conclusions

In the AFm phases containing interlayer water molecules, major changes in the volume discontinuity take place at ~2.0 GPa hydrostatic

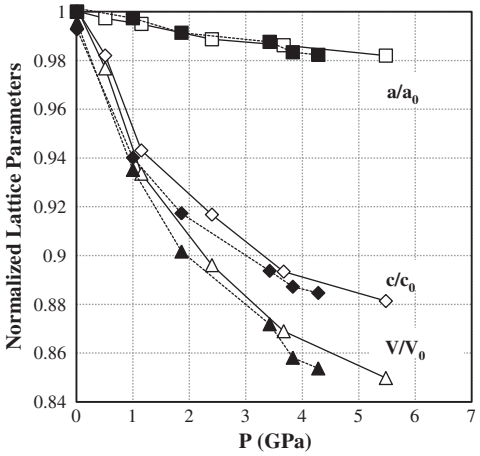

Fig. 7. Unit cell parameters and volume of hemicarboaluminate normalized to ambient values as a function of pressure. Closed and open symbols correspond to pressure medium of 4:1 methanol:ethanol and silicone oil, respectively.

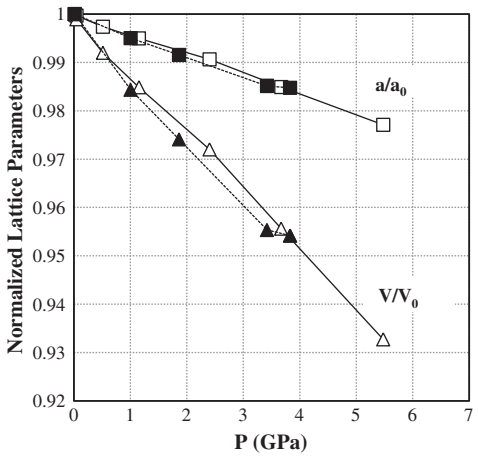

Fig. 9. Unit cell parameters and volume of hydrogarnet normalized to ambient values as a function of pressure. Closed and open symbols correspond to pressure medium of 4:1 methanol:ethanol and silicone oil, respectively.

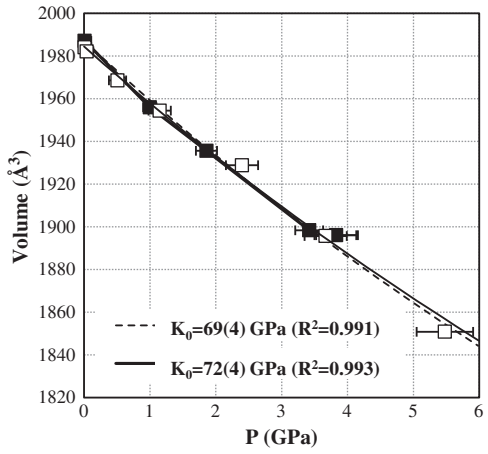

Fig. 10. Unit cell volume as a function of pressure fitted to the B.M. EoS for hydrogarnet. K_o' is fixed at 4.0. Closed symbols with a dotted line and open symbols with a solid line correspond to pressure medium of 4:1 methanol:ethanol and silicone oil, respectively.

pressure, regardless of the type of pressure-transmitting medium. The sudden changes of the c-lattice parameter are in good agreement with the previous studies of the layer thickness of different hydration stages caused by temperature variation. In the case of hemicarboaluminate, the re-orientation of perpendicular direction of planar carbonate group could influence its sudden volume contraction although the experimental results seem to indicate that the pressure-induced dehydration is the prevalent mechanism especially with a hygroscopic pressure medium. This pressure-induced dehydration caused significant changes in the bulk modulus so a two stage bulk modulus was calculated. The bulk moduli of AFm phases are significantly different, depending on the number of interlayer water molecules and the type of anion species.

Acknowledgements

This publication was based on work supported in part by Award No. KUS-l1-004021, made by King Abdullah University of Science and Technology (KAUST). The Advanced Light Source is supported by the Director, Office of Science, Office of Basic Energy Sciences, of the U.S. Department of Energy under Contract No. DE-AC02-05CH11231.

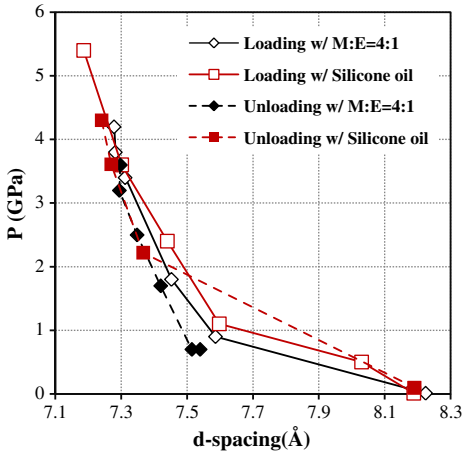

Fig. 11. Layer thickness of hemicarboaluminate as a function of pressure. Black and red lines correspond to pressure medium of 4:1 methanol:ethanol and silicone oil, respectively. Open symbols with solid lines and closed symbols with dot lines correspond to loading and unloading data points, respectively.

Table 4
Experimental and computed equilibrium lattice parameters, bulk modulus, and its derivative for hydrogarnet.

		a (Å)	V (Å^3)	K_o'	K_o (GPa)
Experiment	Powder X-ray diffraction[a]	12.57	1985.9 (3)	4.1(5)	66(4)
	Neutron powder diffraction[b]	12.57	1985(3)	4	52(1)
	Single-crystal X-ray diffraction[c]	12.57	1987.6 (1)	4.0(7)	58(1)
	This study (alcohol mixture)	12.57(1)	1987.11 (1)	4 (fixed)	69(4)
	This study (silicone oil)	12.57(7)	1984.51 (7)	4 (fixed)	72(4)
Calculation	*Ab initio* simulation[d]	12.65	2021.8	3.6(1)	56(1)
	Ab initio Hartree-Fock Hamiltonian[e]	12.71	2051.8	4.1	67
	Ab initio B3-LYP Hamiltonian[e]	12.65	2024.2	4	68

Note: [a]B.M. first order, alcohol mixture [16]. [b]B.M. second order, oil pressure[17]. [c]B.M. third order, 4:1 methanol:ethanol mixture[18]. [d]B.M. third order[19]. [e]B.M. third order [20].

References

[1] H.F.W. Taylor, Crystal structures of some double hydroxide minerals, Mineralogical Magazine 39 (1973) 377–389.
[2] R. Allman, Chimica 24 (1970) 1970.
[3] H.F.W. Taylor, Cement Chemistry, 2nd editionThomas Telford, London, 1997.
[4] G. Hentschel, H.J. Kuzel, Strätlingite, $2CaO–Al_2O_3–SiO_2.8H_2O$, ein neues Mineral, Neues Jahrbuch für Mineralogie Monatshefte (1976) 326–330.
[5] H.J. Kuzel, Crystallographic data and thermal decomposition of synthetic gehlenite hydrate $2CaO·Al_2O_3$ SiO_2 8H2O, Neues Jahrbuch für Mineralogie Monatshefte 3 (1976) 319–325.
[6] M. Balonis, F. Glasser, The density of cement phases, Cement and Concrete Research 39 (2009) 733–739.
[7] R. Rinaldi, M. Sacerdoti, E. Passaglia, Strätlingite: crystal structure, chemistry, and a reexamination of its polytype vertumnite, European Journal of Mineralogy 2 (1990) 841–849.
[8] S. Kwan, J. LaRosa, M.W. Grutzeck, ^{29}Si and ^{27}Al MASNMR study of strätlingite, Journal of the American Ceramic Society 78 (1995) 1921–1926.
[9] H.G. Midgley, P.B. Rao, Formation of Strätlingite, $2CaO·SiO_2$ Al_2O_3 $8H_20$, in relation to the hydration of high alumina cement, Cement and Concrete Research 8 (1978) 169–172.
[10] R. Fischer, H.J. Kuzel, Reinvestigation of the system $C_4A·nH_2O–C_4A·CO_2·nH_2O$, Cement and Concrete Research 12 (1982) 517–526.
[11] G. Renaudin, M. Francois, O. Evrard, Order and disorder in the lamellar hydrated tetracalcium monocarboaluminate compound, Cement and Concrete Research 29 (1999) 63–69.
[12] S.M. Clark, B. Colas, M. Kunz, S. Speziale, P.J.M. Monteiro, Effect of pressure on the crystal structure of ettringite, Cement and Concrete Research 38 (2008) 19–26.
[13] H.J. Kuzel, Uber die orientierte entwässerung von tricalciumaluminathydrat $3CaO·Al_2O_3·6H_2O$, Neues Jahrbuch für Mineralogie Monatshefte (1969) 397–404.
[14] E. Brandenberger, Kristallstrukturelle Untersuchungen an Ca-Aluminathydraten, Schweizerische Mineralogische und Petrographische Mitteilungen 13 (1933) 569, (abstract).
[15] G.A. Lager, T. Armbruster, J. Faber, Neutron and X-ray diffraction study of hydrogarnet $Ca_3Al_2(O_4H_4)_3$, American Mineralogist 72 (1987) 756–765.
[16] H. Olijnyk, E. Paris, C.A. Geiger, Compressional study of katoite $[Ca_3Al_2(O_4H_4)_3]$ and grossular garnet, Journal of Geophysical Research 96 (1991) 14313–14318.
[17] G.A. Lager, R.B.V. Dreele, Neutron powder diffraction study of hydrogarnet to 9.0 GPa, American Mineralogist 81 (1996) 1097–1104.
[18] G.A. Lager, R.T. Downs, M. Origlieri, R. Garoutte, High-pressure single-crystal X-ray diffraction study of katoite hydrogarnet: evidence for a phase transition from *Ia3d–I43d* symmetry at 5 GPa, American Mineralogist 86 (2002) 642–647.
[19] R.H. Nobes, E.V. Akahmatskaya, V. Milman, J.A. White, B. Winkler, C.J. Pickard, An ab initio study of hydrogarnets, American Mineralogist 85 (2000) 1706–1715.
[20] F. Pascale, P. Ugliengo, B. Civalleri, R. Orlando, P. D'Arco, R. Dovesi, The katoite hydrogarnet Si-free $Ca_3Al_2([OH]_4)_3$: a periodic Hartree-Fock and B3-LYP study, Journal of Chemical Physics 121 (2004) 1005–1013.
[21] T. Matschei, B. Lothenbach, F.P. Glasser, The AFm phase in Portland cement, Cement and Concrete Research 37 (2007) 118–130.
[22] M. Kunz, A.A. MacDowell, W.A. Caldwell, D. Cambie, R.S. Celestre, E.E. Domning, R.M. Duarte, A.E. Gleason, J.M. Glossinger, N. Kelez, D.W. Plate, T. Yu, J.M. Zaug, H.A. Padmore, R. Jeanloz, A.P. Alivisatos, S.M. Clark, A beamline for high-pressure studies at the Advanced Light Source with a superconducting bending magnet as the source, Journal of Synchrotron Radiation 12 (2005) 650–658.
[23] H.K. Mao, J. Xu, P.M. Bell, Calibration of the Ruby Pressure Gauge to 800 kbar under quasi-hydrostatic conditions, J Geophys Res 91 (1986) 4673–4676.
[24] A.P. Hammersley, S.O. Svensson, M. Hanfland, A.N. Fitch, D. Hausermann, Two-dimensional detector software: from real detector to idealised image or two-theta scan, High Pressure Research 14 (1996) 235–248.

[25] R.W. Cheary, A.A. Coelho, Programs XFIT and FOURYA, Deposited in CCP14 Powder Diffraction Library, Engineering and Physical Sciences Research Council, Daresbury Laboratory, Warrington, England, 1996, http://wwwccp14acuk/tutorial/xfit-95/xfithtm.
[26] J. Laugier, B. Bochu, CELREF. Version 3. Cell parameter refinement program from powder diffraction diagram, Laboratoire des Matériaux et du Génie Physique, Ecole Nationale Supérieure de Physique de Grenoble (INPG), France, 2002.
[27] F. Birch, Finite strain isotherm and velocities for single-crystal and polycrystalline NaCl at high pressures and 300 K, Journal of Geophysical Research 83 (1978) 1257–1268.
[28] B.C. Reed, Linear least-squares fits with errors in both coordinates, American Journal of Physics 57 (1989) 642–646.
[29] R. Jeanloz, Finite-strain equation of state for high-pressure phases, Geophysical Research Letters 8 (1981) 1219–1222.
[30] R.M. Hazen, Zeolite molecular sieve 4A: anomalous compressibility and volume discontinuities at high pressure, Science 219 (1983) 1065–1067.
[31] M. François, G. Renaudin, O. Evrard, A cementitious compound with composition $3CaO \cdot Al_2O_3 \cdot CaCO_3 . 11H_2O$, Acta Crystallographica Section C 54 (1998) 1214–1217.